00.11

# Probing Multiple Melting Behavior in Poly(ethylene naphthalene-2,6-dicarboxylate) Samples with a Different Thermal History by Simultaneous Wide and Small-angle X-ray Scattering

Z. DENCHEV[†], A. NOGALES, I. ŠICS[‡], T. A. EZQUERRA[*], F. J. BALTÁ-CALLEJA

Instituto de Estructura de la Materia, CSIC, Serrano 119, 2806 Madrid, Spain

Journal of Polymer Science: Part B: Polymer Physics

Revised version: January 2001

[*] To whom correspondence should be addressed (e-mail: imte155@iem.cfmac.csic.es)

[†] Permanent address: University of Minho, Department of Polymer Engineering, Guimarães - 4800-038, Portugal

[‡] Permanent address Riga Technical University, Institute of Polymer Materials, Latvia

## SYNOPSIS

A simultaneous wide and small angle X-ray scattering study of two poly(ethylene naphthalene 2,6-dicarboxylate) (PEN) samples crystallized from the glassy state at different annealing temperature ($T_a$) for different annealing times ($t_a$) was carried out using synchrotron radiation. Either single or dual melting was induced in the samples as confirmed by differential scanning calorimetry (DSC). The correlation function (CF) and the interface distribution function (IDF) were calculated to evaluate the microstructural parameters such as the long spacing, the thickness of the amorphous and crystalline phases, as well as the width of the size distributions. It is demonstrated that the sample with dual melting behavior exhibits an abrupt increase of all microstructural parameters at temperatures above the melting of the lowest endotherm, while the sample revealing a single melting endotherm does not show such a sudden change. This finding is in accordance with the concept that the appearance of two melting peaks in the DSC traces can be explained by the dual lamellar stacking model.

*Key words*: PEN, DSC, dual melting, correlation function, interface distribution function

## INTRODUCTION

The occurrence of single, dual or multiple melting peaks in the differential scanning calorimetry (DSC) traces of polymers during heating is a long time well known and intensively studied phenomenon[1,2]. It is now agreed that a better understanding of the origin of the melting behavior can provide a useful knowledge about the evolution of structure and morphology in the corresponding polymer as a function of temperature[3].

Although the DSC technique provides some insights about morphology, it does not yield a direct morphological information. Other methods such as small-angle X-ray scattering (SAXS) and wide-angle X-ray scattering (WAXS), are often employed in addition to the calorimetric ones[2-11]. Abundant X-ray scattering data have been collected, especially for some of the so-called semirigid polymers – poly(ethylene terephthalate) (PET)[4-7], poly(ether ether ketone) (PEEK)[2,8-11] and to a smaller extent for poly(naphthalene 2,6-dicarboxylate) (PEN)[10]. Several models[3] have been proposed to account for the melting behavior in these polymers but none of them is entirely compatible with all physical observations often being quite controversial. Only the dual lamellar stack model, originally proposed by Cebe and Hong[12] and Basset et al.[13] has not been directly refuted so far[3]. According to this model, in a semicrystalline polymer, both, thick and thin lamellae coexist (also called primary and secondary lamellae, respectively), either located in different stacks or packed within the same stack. Very recent structural investigations by Marand et al[14] bring forward new results favoring the concept of a more or less parallel disposition of macromolecules within the secondary lamellar stacks ("fringed micellar crystals"), rather than of being folded as represented by the well-known chain-folding model.

In a preceding paper[15], the dual lamellar stack model was used to correlate the microstructural data of various PEN samples crystallized from the glass, to the number and shape of their melting endotherms. A direct connection between the DSC endothermic behavior and the microstructure of different PEN samples as revealed by simultaneous WAXS and SAXS (WSAXS) performed at 50°C was found.

The aim of the present study is to examine the influence of the temperature upon the microstructural changes in two different, well-defined, PEN samples exhibiting either single or dual melting behavior. In the present investigation, we provide additional evidence for the applicability of the dual lamellar stack model in samples displaying double melting endotherms in their DSC traces.

## EXPERIMENTAL

### *Materials*

The PEN used in this study (Eastman Chemicals, ref. No PLS 14991) was in the form of pellets with a viscosity-average molecular weight $\bar{M}_v$ = 25.000. Fully amorphous PEN films with a thickness of about 0.2 mm were prepared by mold pressing and quenching as previously described[15]. This procedure could be summarized as follows. The PEN pellets were firstly dried in vacuum for 24 h at 100°C. Subsequently, they were pressed at 300°C for 2-3 minutes and then quenched to room temperature within 20-30 sec. by letting cold water pass through the pressing plates. To perform cold crystallization experiments, amorphous PEN films were introduced into a tightly closing stainless steel chamber that was placed into a vacuum oven. Two PEN samples with varying WAXS crystallinities were then produced by crystallization from the glass (cold crystallization) performed in vacuum under the conditions indicated in Table 1. The melting behavior of

the samples was found to be highly dependent on the annealing conditions employed, namely annealing time ($T_a$) and annealing temperature ($t_a$).

***Techniques***

The DSC traces were obtained in an indium calibrated Perkin-Elmer DSC-7 instrument at a heating rate of 10 deg.min$^{-1}$ in a dry nitrogen atmosphere. Sample weights varied typically in the 8-10 mg range.

WSAXS measurements while heating the samples in the 50-300°C range at a heating rate of 10 deg.min$^{-1}$ were performed in the A2 beamline at HASYLAB (Hamburg, Germany). The wavelength of the pinhole collimated X-rays from the synchrotron source was 0.15 nm. The setup for simultaneous WAXS and SAXS measurements employed is schematically presented in Fig.1. The polymer sample was introduced into the temperature cell (Fig. 1, position 1), and the latter was placed in an evacuated chamber (pos. 2). The scattered X-ray radiation was monitored by two gas-filled, position sensitive detectors – for SAXS (3), and for WAXS (4), respectively. The pathway of the radiation scattered at small angles (6) was evacuated. For most of the SAXS experiments, the sample (1) to detector (3) distance was set at 1450 mm. Some measurements were performed changing the said distance to 2090 mm. All SAXS patterns were normalized with respect to the primary beam. This enables comparison of the scattering intensities in patterns of one and the same sample obtained at various temperatures. The angular range for the WAXS measurements was $13° < 2\theta < 31°$. In both WAXS and SAXS measurements an acquisition time of 10 sec was used for every data frame with a 3 sec waiting time between the patterns. The heating rate in the temperature range from 50 to 300°C was 10 deg$^{-1}$.

To process the SAXS output data and calculate the long spacings ($L$), amorphous- ($l_a$) and crystal phase ($l_c$) thicknesses as a function of the temperature, OTOKO[16] and SASDAP[17] software were employed. By means of the latter, all SAXS profiles were analyzed by a combination of correlation function $\gamma_{1,r}$ (CF) (Eq. 1) and interface distribution function $g_{1,r}$ (IDF) methods (Eq. 2):

$$\frac{\gamma_{1,r}}{Q} = \frac{\int_0^\infty (I - I_b) q^2 \cos(qr) \exp(\sigma^2 q^2) \mathrm{d}q}{\int_0^\infty (I - I_b) q^2 \mathrm{d}q} \tag{1}$$

$$\frac{g_{1,r}}{Q} = \frac{\int_0^\infty G_q \cos(qr) \exp(\sigma^2 q^2) \mathrm{d}q}{\int_0^\infty (I - I_b) q^2 \mathrm{d}q} \tag{2}$$

In Eqs. 1 and 2, $q = (4\pi/\lambda)\cdot\sin\theta$ is the scattering vector and $2\theta$ is the scattering angle. $I_b$ represents that contribution to the total scattering arising from density fluctuations (also called "liquid scattering"), and $\sigma$ is a term, related to the thickness of the crystal/amorphous interface. Q is the scattering power (or scattering invariant) that can be determined by integrating the SAXS profile over all scattering angles, *i.e.*:

$$Q = \int_0^\infty (I - I_b) q^2 \mathrm{d}q \tag{3}$$

When considering the structure of an ideal two-phase model, Q can then be related to the following morphological variables[9]:

$$Q = k x_{sph} x_{st} \frac{l_c}{l_c + l_a} \frac{l_a}{l_c + l_a} (\rho_c - \rho_{ila})^2 \tag{4}$$

Here, $k$ is a calibration constant, $x_{sph}$ is the volume fraction of the spherulites in the material, $x_{st}$ is the volume fraction of lamellar stacks within the spherulite, $\rho_c$ and $\rho_{ila}$ are the electron densities in the two phases – crystalline and interlamellar, respectively.

The $G_q$ term in Eq.(2) characterizes the interference function of the two-phase system:

$$G_q = K - (I - I_b)q^4 \exp(\sigma^2 q^2) \tag{5}$$

wherein $K$ stands for the Porod constant.

One can obtain two estimates for $L$ from CF if one considers either the position of its first maximum ($L_c^M$) or from twice the position of the first minimum ($L_c^m$). The first minimum of IDF gives one more set of long spacing values denoted further by $L_I$. Additional analysis of both CF and IDF provides values for $l_c$ and $l_a$. More details about the theoretical background and practical performance of these calculations can be found elsewhere[9,15,18,19].

SASDAP gives one more estimate for $L$, namely the Bragg long period ($L_B$) as derived from $q_{max}$ of the Lorentz corrected SAXS pattern in accordance with Eq. 6:

$$L_B = \frac{2\pi}{q_{\max}} \tag{6}$$

## RESULTS

### *DSC measurements*

Fig. 2*a* displays the DSC curve (solid line) of an originally amorphous PEN sample annealed for $t_a$ = 4 hours at $T_a$ = 240°C. A well-expressed single melting endotherm is obtained, with a peak value of 266°C (Table 1). The sample annealed at $t_a$ = 24 h and $T_a$ of 165°C reveals a double melting behavior (Fig. 2*b*, solid line). The peak value of the first, low intensity endotherm is located at 185°C, and that of the second endotherm lies at 268°C. Closer inspection of the 240-260°C region reveals a small but measurable crystallization around 240°C followed by the broad "nominal" melting peak.

Fig. 2 shows also the temperature dependence of the Q-values (dashed lines) of the two samples under investigation. The evolution of the Q curve for the sample with

the single melting behavior (2*a*) is characterized by a relatively small and gradual increase. This increase starts at about 120°C and, without a measurable change of the slope, goes up to about 266°C. At this temperature an abrupt drop in the Q-values is observed, this trend remaining unchanged until the complete melting of the sample as indicated by DSC. The Q-value of the sample with the dual melting behavior (2*b*) changes in a more complex way. The increase of Q is steeper, the slope of the curve changing several times: around 120°C, close to 200°C and at 247°C. At the latter temperature, *i.e.*, more than 20°C below the maximum of the second melting endotherm in the DSC traces, Q abruptly and irreversibly decreases.

***WAXS measurements***

Selected WAXS patterns of both PEN samples obtained in the temperature range between 50-300°C are presented in Fig. 3*a* and 3*b*. For better visualization, stacked plots are presented, the curves being gradually displaced from one another in upward direction. Irrespective of the annealing conditions, the WAXS traces are all consistent with the $\alpha$-modification of the unit cell characterized by a strong [010] reflection. Another common feature to both samples is that the WAXS reflections are observed for all temperatures within the interval between the onset and offset temperatures of the DSC peaks (Table 1, Fig. 3*a* and 3*b*). The scattering intensity of the patterns gradually diminishes with the increase of temperature. In addition to this general trend in sample 2, a change in the intensity of the [010] reflection was observed in the 200-250°C range.

***SAXS measurements***

The most characteristic SAXS profiles for both samples are presented in Fig. 4. For the sample with the single melting behavior (Table 1, No 1), well defined SAXS

scattering maximums with increasing intensity and similar long spacing values were registered in the 50-265°C interval (Fig. 4*a*). The location of the maximum of the curve obtained at 270°C is not immediate without additional deconvolution (Lorentz correction) since it is partially overlapped by the primary beam. No scattering peak was registered at 274°C.

The second sample in Table 1 is characterized in the 50-200°C range by scattering peaks of lower intensities; however, a sharp intensity increase was observed above 200°C (Fig. 4*b*). This effect is accompanied by a shift of the peak maximums to smaller values of the scattering vector. At 262°C the scattering peak is not anymore detectable, most probably because the primary beam peak is masking it. The intensity of the pattern at 262°C increases by a factor 7, as compared to that taken at 195°C. At 274°C the sample shows no discrete small-angle scattering maximum.

***Determination of L, $l_a$ and $l_c$ from the correlation function***

Figs. 5*a* and 5*b* (bottom graphs) display the temperature dependence of the long spacings calculated from the Lorentz-corrected Bragg peak maximums ($L_B$), from CF ($L_c^M$ and $L_c^m$), and from the IDF ($L_I$). The upper graphs in these figures represent the same dependence of the crystal and amorphous layer thicknesses as derived from CF ($l_c^{CF}$, $l_a^{CF}$) and IDF ($l_a^{IDF}$), respectively.

The crystalline thickness in both samples was attributed to the more abundant phase (or, larger thickness) within the stacks because of the following reasons. As seen from Table 1, the average volume crystallinity of Sample 1 ($T_a$ = 240°C) is significantly higher than that of Sample 2 ($T_a$ = 165°C), while their $x_I$ values are almost the same (0.69 and 0.71, respectively). On the other hand, both $\chi_c^{vol}$ fractions in Table 1 (0.48 and 0.33, respectively) are significantly lower than the corresponding $x_I$ values. It seems

logical that for both Sample 1 and Sample 2 the $x_1$ values would correspond to the crystal fractions within the stack. The physical meaning of this assumption could be that there is a certain amount of amorphous material outside the stacks in which these are embedded, that is, the microstructure will be in agreement with the lamellar stack model. The other option (*i.e.*, association of $x_1$ with the amorphous phase) would mean that the linear crystallinity within the stack is lower than the average sample crystallinity which apparently has no physical meaning. One may also assume, that in Sample 2 with $T_a$ = 165°C the interstack amorphous regions are larger then those within the stacks [15].

We applied the CF and IDF formalisms only where a clear peak was present in the raw SAXS profiles of the samples (Fig. 4). Since all the $L$ values show a similar variation with temperature, whenever discussing absolute values, unless otherwise specified, we will refer to $L_c^M$.

The data presented in Fig. 5*a* and Table 2 for PEN with one single melting peak (sample 1), show a slight increase of $L$ in the 100 and 270°C range. The largest $L$ value of 148 Å is recorded at 270°C. *i.e.*, immediately before the complete melting of the sample. Measurements above 270°C were not considered since no coherent scattering above this temperature is observed.

For sample 2, relatively constant values of $L$, $l_a$ and $l_c$ are observed when increasing the temperature from 100°C up to 190-200°C. However, a significant increase of these parameters is detected in the temperature range between 200 and 255°C. Here, both $l_c$ and $l_a$ values grow markedly, to give an $L$ value at 240°C larger (about 35 Å) than that at 100°C. Above 240°C the increasing rate of the parameters becomes even higher, their last reliable values at 255°C being $L$ = 159 Å, $l_c$ = 109 Å, $l_a$ = 50 Å. The measurements above this temperature are related to the peak of the primary beam that

completely overlaps any scattering. Therefore, we do not discuss the temperature range enclosed between 260 and 300°C.

***Interface distribution function analysis***

Figs. 6*a* and 6*b* show the IDF temperature dependence from 100°C up to 270°C (last temperature at which a scattering peak was recorded in both raw SAXS profiles). In Sample 1 (Fig. 6*a*, single melting endotherm in DSC), the positive part of the IDF broadens gradually and only slightly with temperature, especially between 250-270°C, this broadening being accompanied by a small upward shift of the first maximum. The sample with the double melting behavior (Fig. 6*b*) displays quite narrow IDF curves up to about 240°C. At this temperature the onset of the higher melting peak, as seen from the DSC traces in Fig. 2 and Table 1, is evident. Furthermore, the width of IDF increases notably within the 242-254°C temperature range, the curves being similar to those corresponding to Sample 1 in the whole temperature range.

## DISCUSSION

***Background***

In a preceding study[15] it was shown that all the DSC traces of cold crystallized PEN with WAXS crystallinity in the range of 5-27%, presented always a melting peak at 260-265°C. However, lower melting endotherm, developed only when the crystallinity grew above 20%. If, as indicated by Krüger and Zachmann[2], the lower endotherm was assigned to the melting of the secondary lamellae, then in our case the primary lamellae would appear *before* the secondary ones. As previously stated[3], such a behavior

disagrees with the melting-recrystallization model. This was one of the reasons to explain the dual melting peak in PEN in terms of the dual lamellar stacking model. On the other hand, a single melting peak in DSC seemed to correspond to a morphology more consistent with the finite lamellar stack model having similar thickness distributions of both phases. All these conclusions were supported by X-ray data obtained at 50°C[15].

The present study extends the above structural investigation to the temperature range of 50-300°C. Our basic assumption is the following: if the DSC dual melting behavior does really correspond to a dual lamellar stack morphology, thus, by increasing the temperature of the SAXS experiment above that of the lower endotherm ($T_m^1$), one should observe $L$ values notably higher than those obtained before the heating ramp. The explanation is that for $T>T_m^1$ the crystals from the secondary lamellar stacks formed during the sample preparation would melt, thereby revealing the size of $L$ in the higher melting lamellae in the primary stacks. Accordingly, if the microstructure of the sample approaches the finite lamellar stack model involving a lower variance of the lamellar sizes, then an increase in temperature at which the SAXS pattern is taken will not significantly affect the values for $L$, $l_a$ and $l_c$.

***Sample 1: Single melting behavior***

In accordance with the above considerations, the PEN sample which shows a single melting endotherm displays a relatively small and gradual increase of the morphological parameters within the whole interval of 100-270°C. Analysis of the corresponding $L$, $l_c$ and $l_a$ values (Table 2) leads to the conclusion that the slight increase of the $L$ values by 18 Å could be attributed to a growth of both $l_a$ and $l_c$. However, the elimination of some smaller, less perfect lamellae could also be possible.

Fig 2*a* shows that for sample 1 the Q-values start growing above 120°C, *i.e.*, above $T_g$, the global maximum $Q_{max}$ coinciding with the temperature of the DSC melting peak. This observation suggests that in sample 1 there are only stacks in which the lamellar thickness and perfection are approximately the same (Fig. 7a). That is why when $T_m^{II}$ is reached the crystalline phase melts instantly causing a simultaneous drop in both DSC and Q-curves.

Another evidence of the assumed microstructure of Sample 1 is supported on the basis of the analysis of the temperature dependence of its IDF (Fig. 6*a*). The analysis of the width and shape of these curves leads to the conclusion of a relatively narrow distribution of sizes for $L$, $l_c$ and $l_a$, at 100°C, that does not change significantly as the temperature of the SAXS measurement increases up to 270°C.

Finally, a comparison of all the estimates for $L$ obtained from the Bragg relation, from the CF and from the IDF functions (Fig. 5*a*) demonstrates the following trend:

$$L_B > L_c^M > L_c^m > L_I. \qquad (7)$$

As shown earlier[15], the above trend implies that the width of the amorphous layer size distribution is larger than that of the lamellar size distribution.

***Sample 2: Dual melting behavior***

The growth of the microstructural parameters of sample 2 at temperatures higher than 200°C (Fig. 5*b*) is in accordance with the supposed melting of stacks containing thinner and less perfect secondary lamellae thus revealing the real size of the primary ones. Fig. 2*b* also yields support for this hypothesis, the $Q_{max}$ value coinciding with the onset of the higher melting endotherm and not with $T_m^{II}$. A possible explanation of this finding is that this sample contains crystalline lamellae characterized by a large variety of crystal sizes and degree of crystal perfection. Some of the lamellae start melting well below $T_m^{II}$, which is reflected by the change in the slope of the Q-values with tempera-

ture above $T_m^I$ (Fig. 7b). The shape of the IDF function at 100°C (Fig. 6*b*) indicates a much broader variance in sizes of the microstructural parameters than the corresponding curve of sample 1, this trend being stable up to 240°C. At higher temperatures (243 and 255°C), there is a notable increase in the width of the IDF curves that is an indication for a narrower distribution of phase sizes.

By analyzing the absolute values for the different estimates of $L$ derived from CF, IDF and Bragg law (Fig.5*b*), one may propose the following trend for Sample 2:

$$L_B > L_c^M > L_I \geq L_c^m. \tag{8}$$

As previously discussed[4,15], the above relation suggests that the variance of the larger thickness values (*i.e.*, that of the crystal lamellae) in sample 2 is larger than the variance of the lower thickness values, the latter being those of the amorphous phase. It is noteworthy that only at temperatures above 240°C $L_I$ becomes equal to $L_c^m$.

The evolution of IDF for sample 2 could be followed up to 255°C. However, above this temperature, no SAXS maximums could be recorded owing to set-up limitations, neither the increase of the sample-to-detector distance to 2090 mm allowed the resolution of a scattering peak.

It is noteworthy that above 240°C the $L$ and $l_c$ values for sample 2 are larger than the corresponding values for Sample 1. At temperatures higher than 265°C, the $L$ and $l_c$ cannot be measured anymore. One possible explanation for this result could be the formation of very thick lamellae. This assumption would require that lamellae thickening and/or intensive recrystallization processes take place above 255°C. Taking into account the temperature dependence of Q (Fig. 2*b*), we are rather inclined to discard such a possibility. Another way to explain the said increase of $L$ and $l_c$ in sample 2 is that close to the melting point of the higher endotherm, the more abundant phase within the lamellar stacks is already the amorphous one. Such an assumption would admittedly explain the

absence of a well-defined peak in their SAXS scattering patterns owing to the presence of very large amorphous regions between the crystalline lamellae, rather than to the presence of very thick lamellae.

## CONCLUSIONS

1. The PEN sample showing a single melting endotherm in the DSC is built up predominantly by primary lamellar stacks with a rather narrow distribution of $L$, $l_a$ and $l_c$.
2. For PEN showing a double melting endotherm, the primary stacks coexist with a significant fraction of secondary stacks containing lamella of diverse size and perfection. During the heating ramp up to 300°C, the secondary lamellar stacks melt in a broad temperature interval above the temperature of the lower melting endotherm. Judging from the analysis of X-ray data, the elimination of secondary stacks is accompanied by melting-recrystallization processes.
3. About 10°C below the melting point, both samples display different absolute values for $L$ and $l_c$ but a similar, relatively narrow distribution of sizes. Most probably, these values characterize the primary lamellar stacks that are the last ones to melt.

## ACKNOWLEDGMENTS

The authors gratefully acknowledge the financial support of DGI FPA2000-0950, Comunidad de Madrid (07N/0063/1998) and DGICYT (Grant PB 94-0049). They are also indebted to B. Hsiao who placed at their disposal the SASDAP software. Z. Denchev gratefully acknowledges the tenure of fellowships awarded by NATO and by the Spanish Ministry of Culture and Education (5B97-K5447945).

## REFERENCES


1) Bernstein, V. A.; Egorov, V. M. Differential Scanning Calorimetry in Polymer Physics, Chemistry: St. Petersburg, 1990, p. 150 (in Russian)

2) Krüger K. N.; Zachmann, H. G. Macromolecules 1993, 26, 5202

3) Verma, R. K.; Hsiao, B. S. Trends in Polymer Science (TRIP) 1996, 4, No9, 312

4) Santa Cruz, C.; Stribeck, N.; Zachmann, H. G.; Baltá-Calleja, F. J. Macromolecules 1991, 24, 5980

5) Jonas, A. M.; Russel, T. P.; Yoon, D. Y. Colloid. Polym. Sci. 1994, 272, 1344

6) Stribeck, N.; Zachmann, H. G, Bayer, R. K., Baltá-Calleja, F. J. J. Mater. Science 1997, 32, 1639

7) Wang, Zhi-Gang; Hsiao, Benjamin; Sauer, Bryan B. Kampert, William G. Polym. Mater. Sci. Eng. 1998, 79, 320

8) Wang, Wu; Schultz, Jerold M.; Hsiao, Benjamin S. J. Macromol. Sci., Phys. 1998 B37(5), 667-682

9) Verma, R. K.; Marand, H.; Hsiao, B. S. Macromolecules 1996, 29, 7767

10) Medellin-Rodriguez, F. J.; Phillips, P. J.; Lin, J. S. Macromolecules 1996, 29, 7491

11) Fougnies, C.; Damman P.; Dosierre M.; Koch, M. H. Macromolecules 1997, 30, 1392

12) Cebe, P.; Hong, S. D. Polymer 1986, 27, 1183

13) Basset, D. C.; Olley, R. H.; Raheil, I. A. M. Polymer 1988, 29, 1745

14) Marand, H.; Alizadeh, A.; Farmer, R.; Desai, R.; Velikov, V. Macromolecules 2000, 33, 3403

15) Denchev, Z.; Nogales, A;, Ezquerra, T. A.; Fernandes-Nascimento, J.; Baltà-Calleja, F. J. J. Polym. Sci., Part B: Polymer Physics 2000, 38, 1167

[16] The OTOKO software is developed by M. H. J. Koch, EMBL - DESY, Notkerstrasse 85, Hamburg, Germany

[17] The SASDAP software (Small Angle Scattering Data Analysis Program) is written by R. Verma in collaboration with A. Biswas and B. Hsiao (all from the Central Research and Development, DuPont Experimental Station, Wilmington, DE, USA)

[18] Baltá-Calleja, F. J.; Vonk, C. G. X-ray Scattering of Synthetic Polymers, Elsevier Science Publishers: New York, 1989; Chapter 7, p.247-265

[19] Hsiao, B. S.; Gardner, K. H.; Wu., D. Q.; Chu, B. Polymer 1993, 34, 3986

**Figure Captions**

**Figure 1** Scheme of the experimental setup for simultaneous SAXS-WAXS experiments at polymer beam-line A2 at HASYLAB-DESY: (1) SAXS-WAXS sample cell, (2) evacuated chamber, (3) SAXS one-dimensional detector, (4) WAXS one-dimensional detector, (5) beam-stop, (6) evacuated optical path.

**Figure 2** DSC curves (solid lines) of initially amorphous PEN films annealed at various conditions: (a) – $T_a$ = 240°C, $t_a$ = 4 h; (b) – $T_a$ = 165°C, $t_a$ = 24 h. For both samples, the temperature dependence of the scattering power Q is given with dashed lines. Heating rate for DSC and X-ray experiments – 10 deg.min$^{-1}$.

**Figure 3** Selected WAXS patterns taken at various temperatures: (a) – sample 1 and (b) – sample 2. Sample designations are according to Table 1. Heating rate = 10 deg.min-$^{1}$ (For more details see the text).

**Figure 4** Selected raw SAXS profiles of the two PEN samples taken at various temperatures: (a) – sample 1 and (b) – sample 2. Heating rate during the synchrotron SAXS measurements – 10 deg.min-$^{1}$.

**Figure 5** Variation of the microstructural parameters as a function of the temperature in: (a) – sample 1 ($T_a$ = 240°C, $t_a$ = 4 h) and (b) – sample 2 ($T_a$ = 165°C, $t_a$ = 24 h). Heating rate – 10 deg.min-$^{1}$. ($L_B$ – long spacing values as computed from Eq. 3; $L_c^m$ and $L_c^M$ – long spacing values calculated from the CF analysis; $L_I$, – long spacing as obtained from IDF in Fig. 6; $l_c$ – thickness of the crystalline phase obtained from the CF analysis; $l_a^{CF}$ – thickness of the amorphous phase from the CF analysis; $l_c^{IDF}$ - thickness of the amorphous phase from he IDF. (For more details see text).

**Figure 6** Temperature dependence of the IDF functions of the two PEN samples with different thermal history and melting behavior: (a) – single DSC peak; (b) dual endothermic behavior (For more details see text).

**Figure 7**. Idealistic and oversimplified model of semicrystalline PEN. Sample (a): single melting, one dominant population of crystalline lamellae (rectangular bars) which melt above $T_m^{II}$; Sample (b) double melting behavior, heterogeneous population of crystalline lamellae [two populations are presented: with thicker (gray bars) and thinner (black bars) crystallites]. The thinner lamellae melt above $T_m^{I}$ and thicker ones – above $T_m^{II}$

**Table 1** Designation and characterization of the PEN samples used for SAXS measurements. ($t_a$ = annealing time; $T_a$ = annealing temperature; $\chi_c^{WAXS}$ - WAXS crystallinity fraction of the initial sample; $\chi_c^{vol}$ - crystallinity fraction obtained by gradient column measurements; $x_1$ = fraction of the phase more abundant in the stack; $(1\text{-}x_1)$ = fraction of the phase less abundant in the stack

| Sample Designation | Annealing conditions | | Crystallinity fraction | | DSC peaks | | | | Phase fractions according to CR [15] | |
|---|---|---|---|---|---|---|---|---|---|---|
| | $t_a$, h | $T_a$, °C | $\chi_c^{WAXS}$ | $\chi_c^{vol}$ | Peak onset, °C | Maximum(s), $T_m^I$; $T_m^{II}$, °C | Peak offset, °C | Melting behavior | $x_1$ | $1\text{-}x_1$ |
| 1 | 4 | 240 | 0.40 | 0.48 | 255 | N/A; 266 | 275 | Single | 0.69 | 0.31 |
| 2 | 24 | 165 | 0.27 | 0.33 | 175, 236 | 185; 268 | 194, 274 | Double | 0.71 | 0.29 |

| | 100°C | 170°C | 190°C | 200°C | 240°C | 247°C | 251°C | 255°C | 265°C | 270°C |
|---|---|---|---|---|---|---|---|---|---|---|
| **Sample 1 $T_a$= 240°C, $t_a$ = 4 h, $R_h$ = 200deg/min** | | | | | | | | | | |
| $L_c^M$, Å | 130 | 136 | 137 | 137 | 141 | 142 | 142 | 142 | 144 | 148 |
| $l_c^{CF}$ Å | 89 | 94 | 95 | 95 | 98 | 96 | 96 | 96 | 96 | 98 |
| $l_a^{CF}$ Å | 41 | 42 | 42 | 42 | 43 | 46 | 46 | 46 | 48 | 50 |
| **Sample 2 $T_a$= 165°C, $t_a$ = 24 h, $R_h$ = 2 deg/min** | | | | | | | | | | |
| $L_c^M$, Å | 103 | 104 | 108 | 109 | 138 | 146 | 152 | 159 | -[a)] | -[a)] |
| $l_c^{CF}$ Å | 71 | 72 | 75 | 76 | 97 | 101 | 104 | 109 | -[a)] | -[a)] |
| $l_a^{CF}$ Å | 32 | 32 | 33 | 33 | 41 | 45 | 48 | 50 | -[a)] | -[a)] |

**Table 2** Evolution of the morphological parameters as a function of the temperature of the X-ray scattering measurement

($L_c^M$ = long spacing as determined from CF; $l_c^{CF}$= crystal layer thickness as determined from CF; $l_a^{CF}$, = amorphous layer thickness as determined from CF)

NOTE: [a)] not measurable, the scattering peak in the raw SAXS profile is overlapped by the primary beam

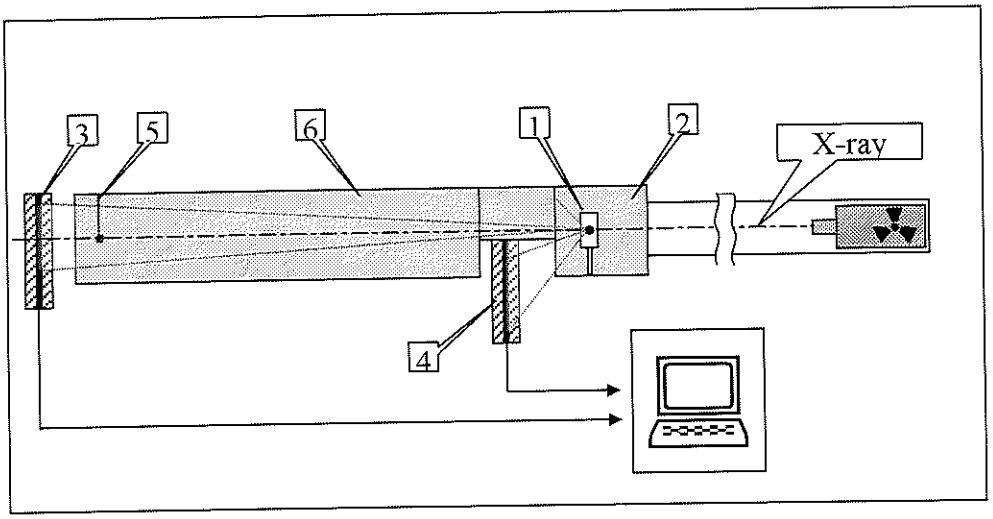


Z. Denchev et al. Figure 1

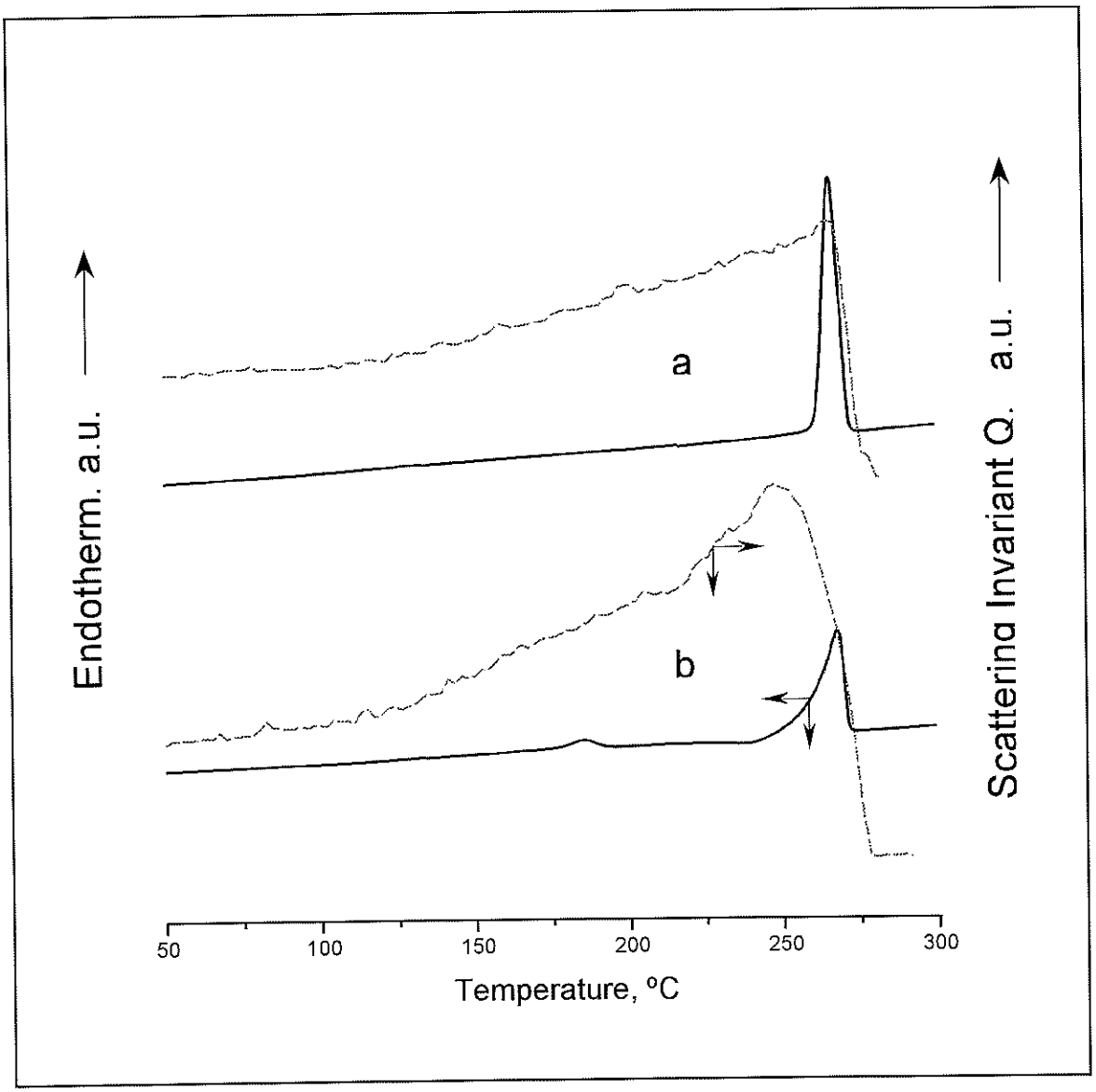


Z. Denchev et a., Fig. 2*a, b*

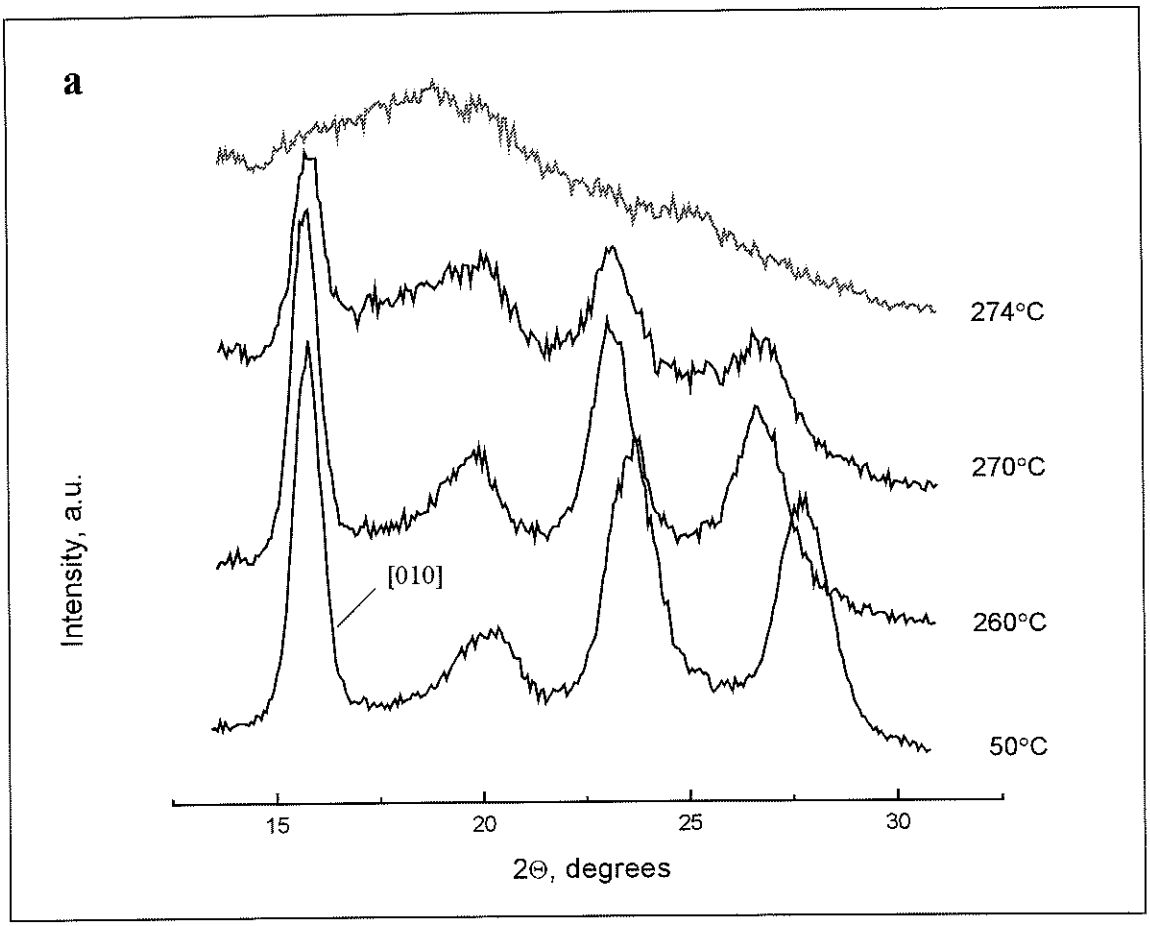


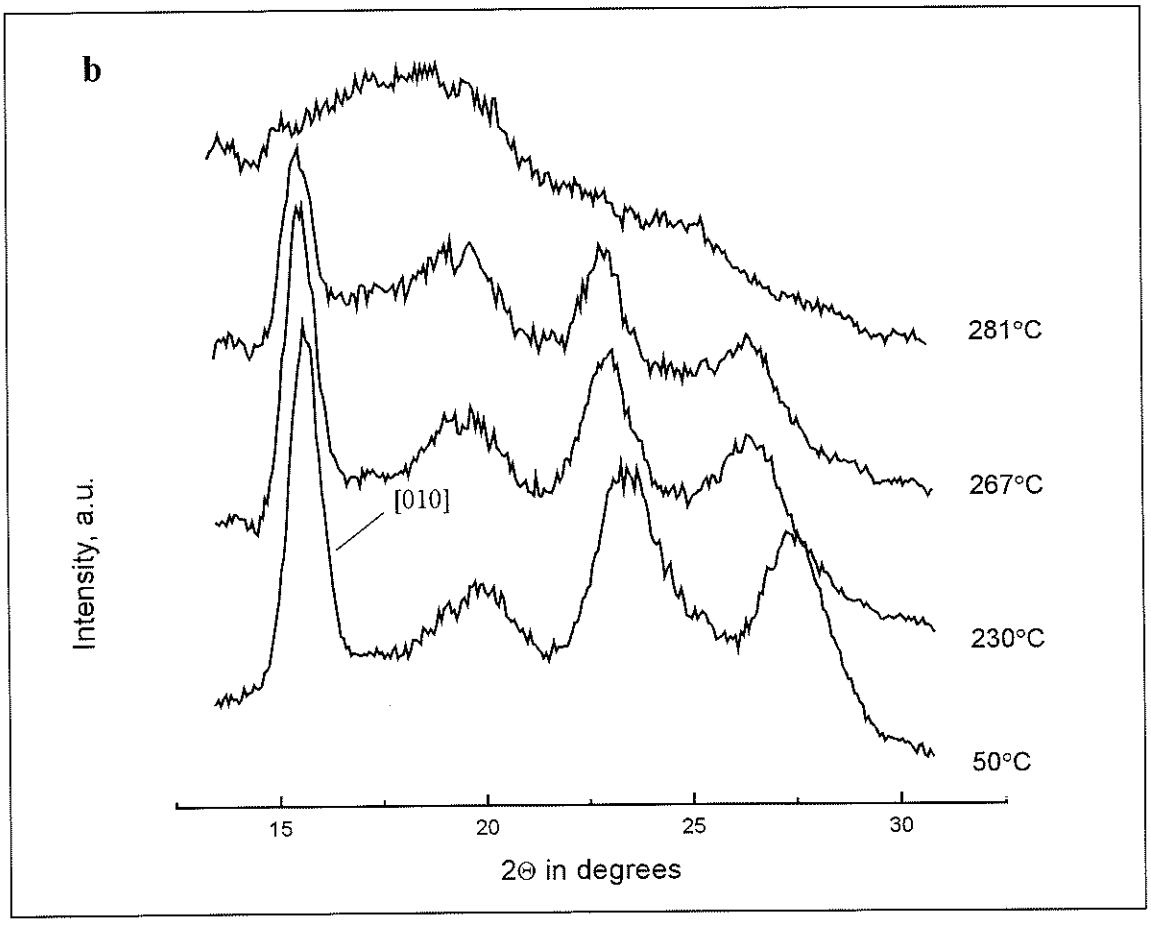


Z. Denchev et. al, Figure 3a, b

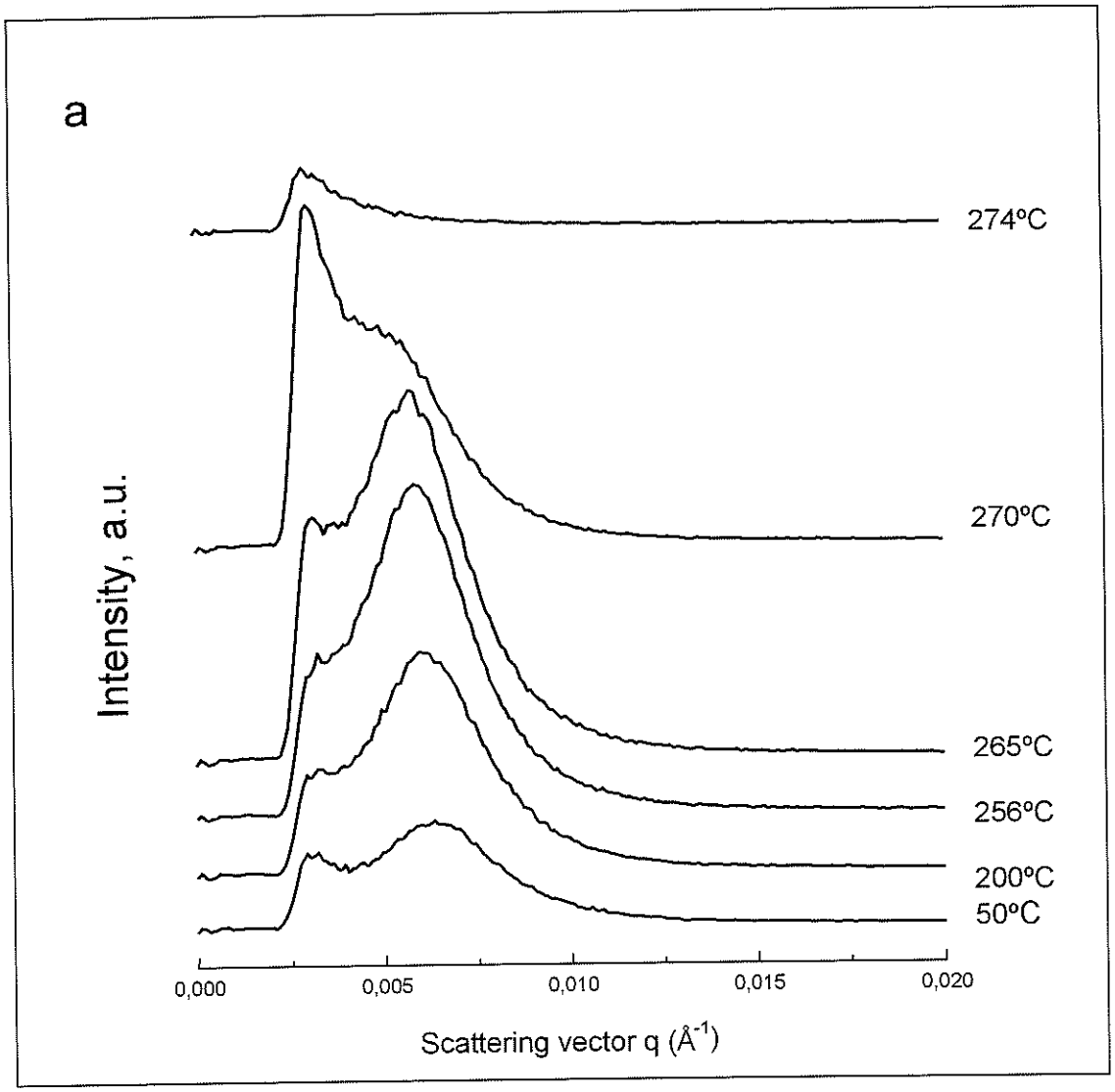


Z. Denchev et al., Figure 4*a*

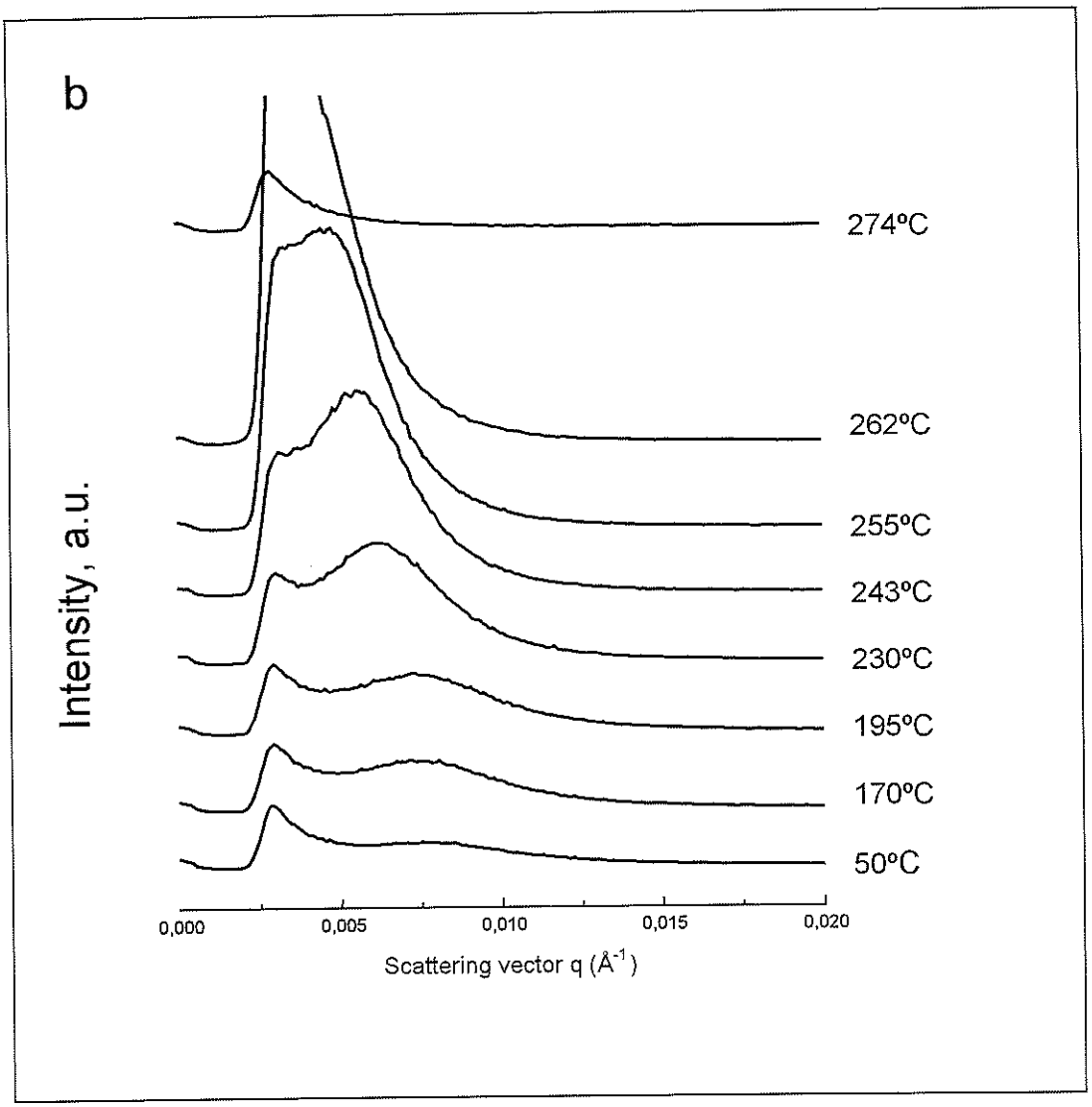


Z. Denchev et al., Figure 4b

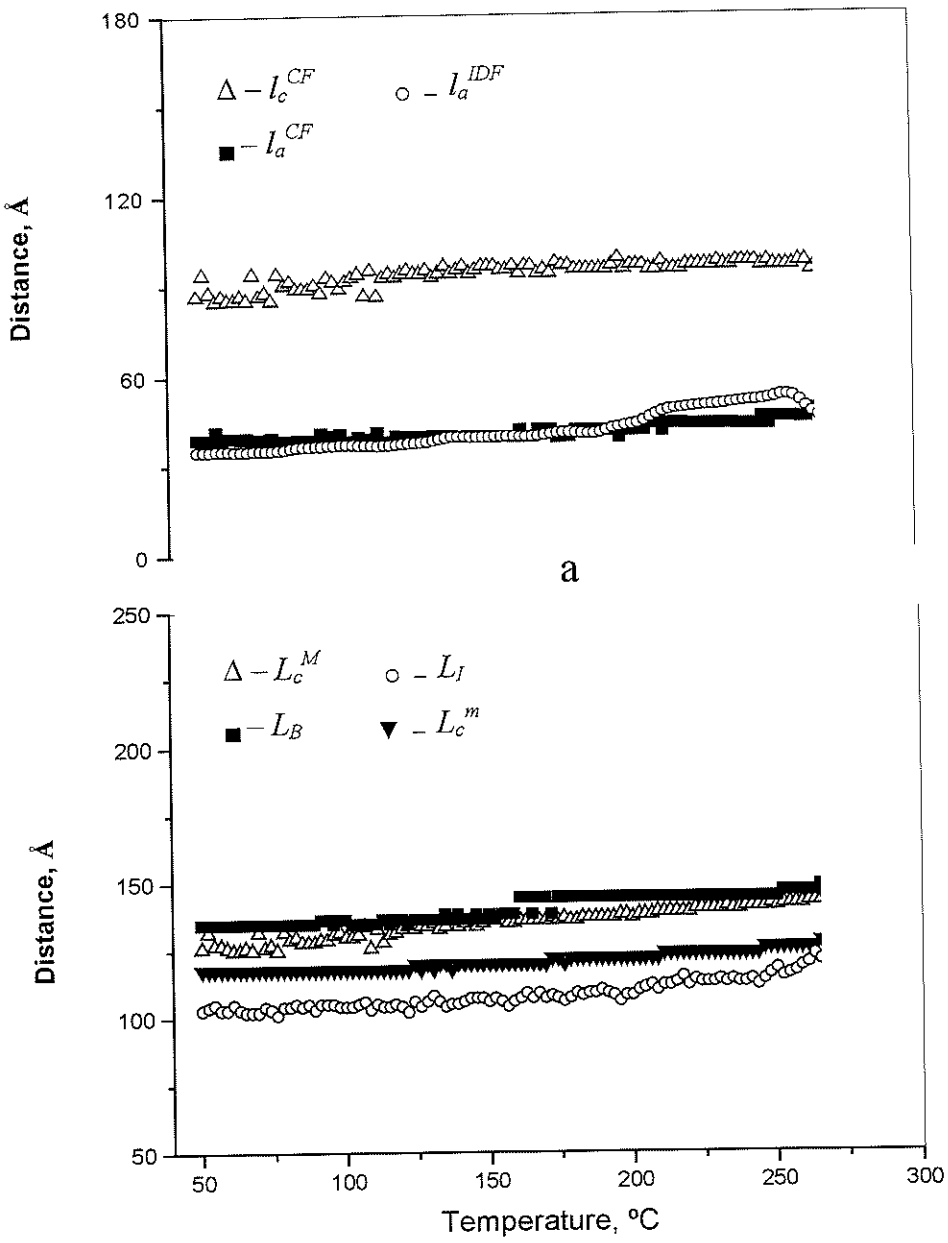


**Figure 5a** Z. Denchev et al.

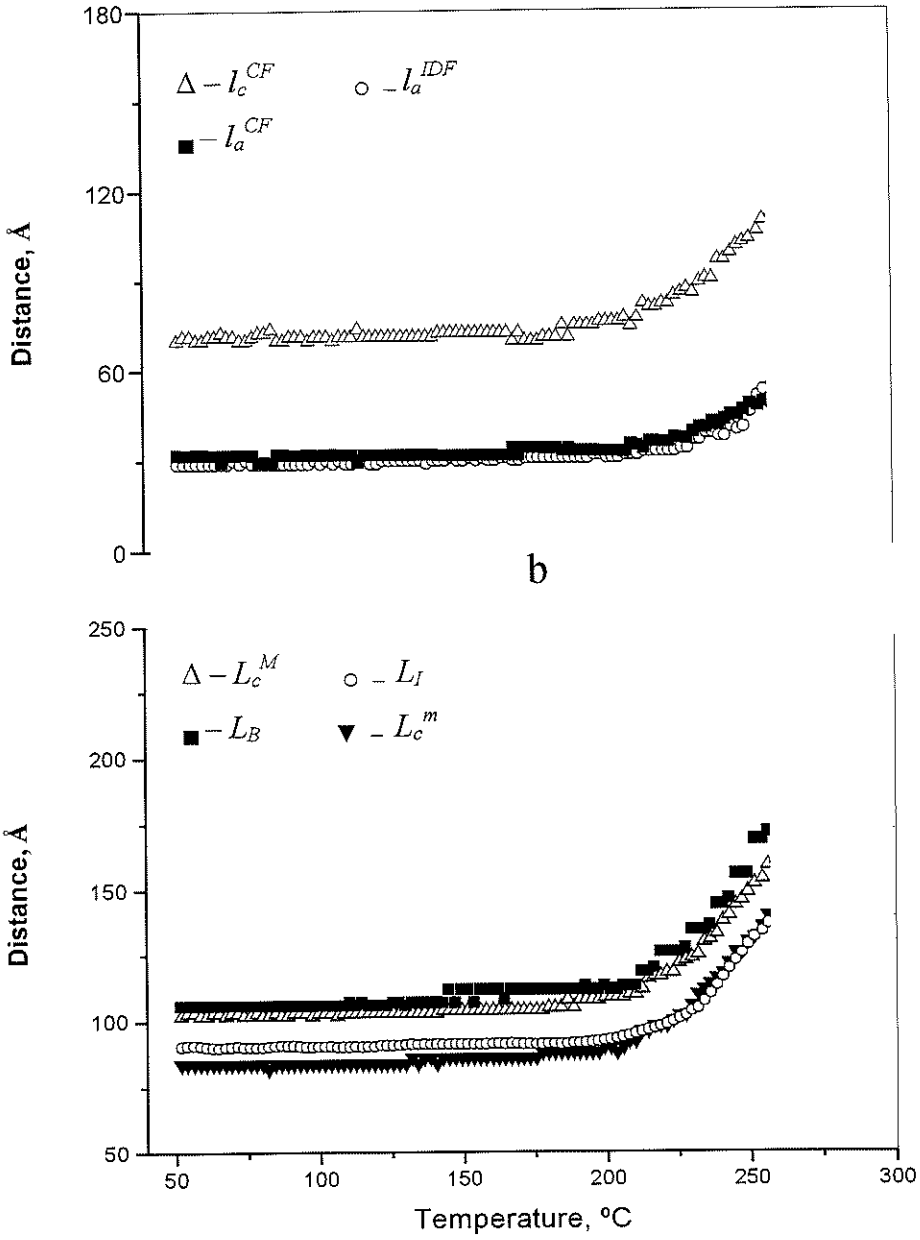


**Figure 5b** Zlatan Denchev et al.

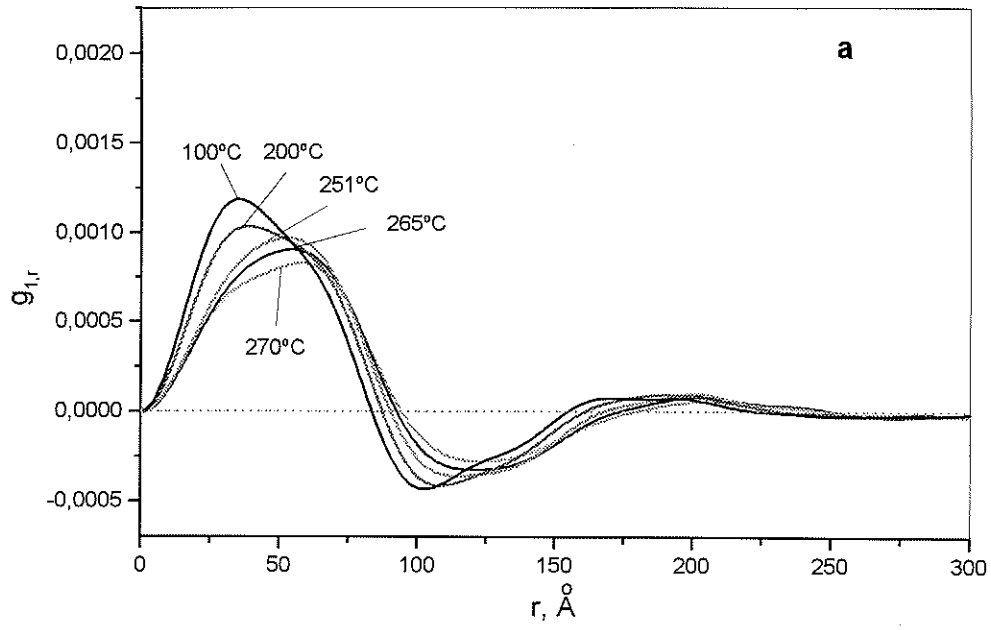


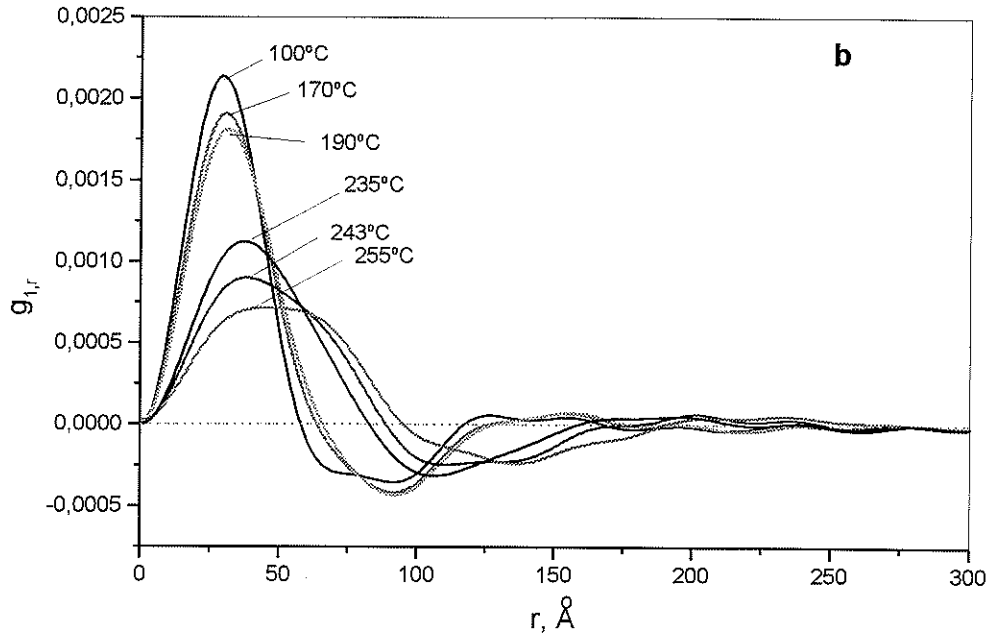


Z. Denchev et al., Figure 6a, b

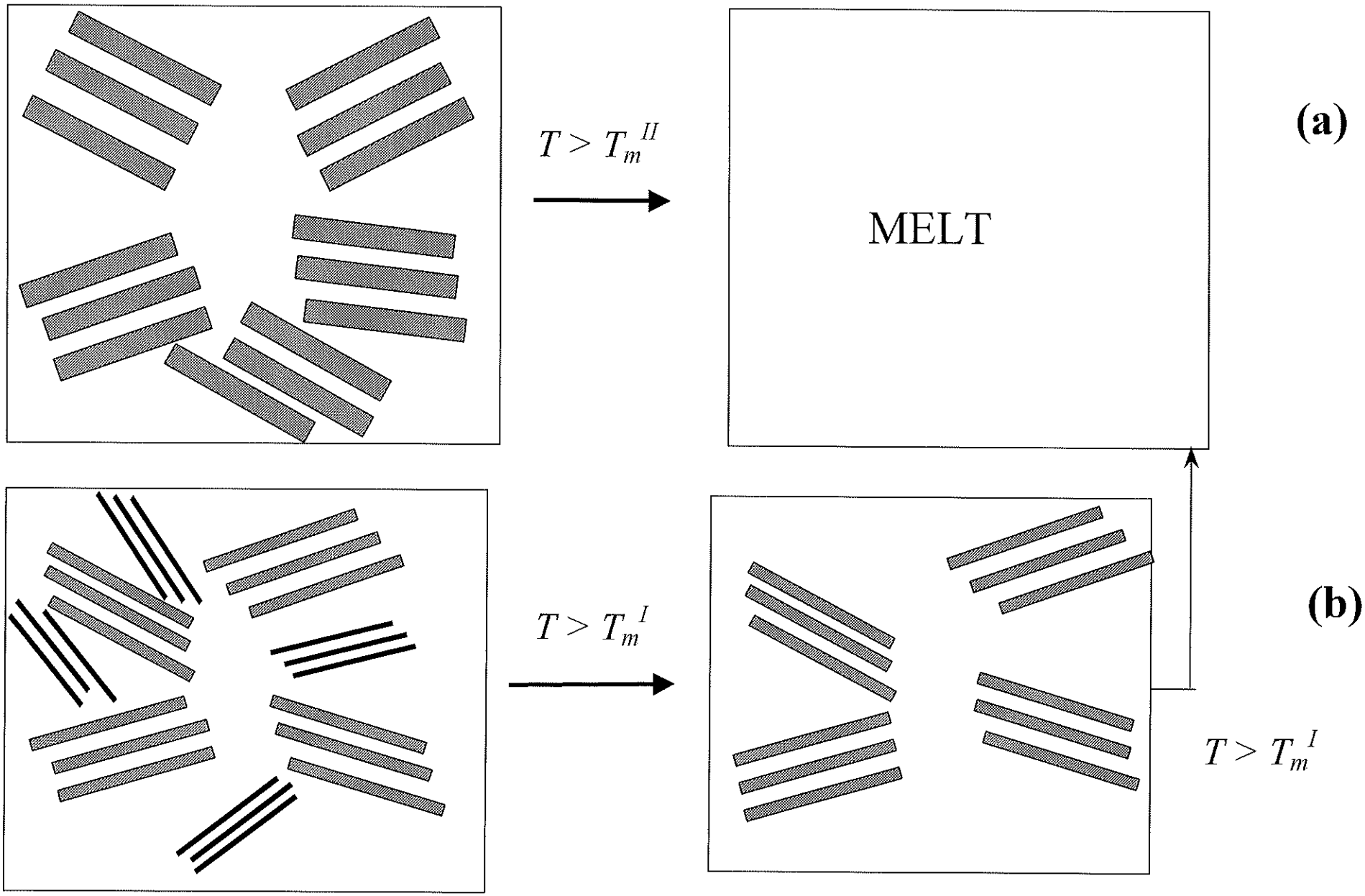
$T > T_m^{II}$
MELT
(a)
$T > T_m^{I}$
(b)
$T > T_m^{I}$